Supporting Information for

Long-Lived $^{13}C_2$ Nuclear Spin States Hyperpolarized by Parahydrogen in Reversible Exchange at Micro-Tesla Fields

*Zijian Zhou[1], Jin Yu[1], Johannes F. P. Colell[1], Raul Laasner[2], Angus Logan[1], Danila Barskiy[3], Roman Schepin[4], Eduard Y. Chekmenev[4], Volker Blum[1,2], Warren S. Warren[1,4] and Thomas Theis[1]**

[1]Department of Chemistry, Duke University, Durham NC 27708, United States

[2]Department of Mechanical Engineering and Materials Science, Duke University, Durham NC 27708, United States

[3]Departments of Radiology, Biomedical Engineering and Physics, Vanderbilt University, Institute of Imaging Science (VUIIS), Nashville, TN 37232, United States

[4]Departments of Radiology, Physics and Biomedical Engineering, Duke University, Durham NC 27708, United States

[1]Department of Chemistry, [2]Department of Mechanical Engineering and Material Science,

[3]Deparment of Physics, Duke University, Durham NC 27708, United States,

[4]Departments of Radiology, Biomedical Engineering and Physics, Vanderbilt University, Institute of Imaging Science (VUIIS), Nashville, TN 37232, United States

[5]Department of Radiology and Biomedical Engineering, Duke University, Durham NC 27708,

United States

AUTHOR INFORMATION

Corresponding Author:

*To whom correspondence should be addressed. E-mail: thomas.theis@duke.edu.

1. Experimental details

1.1 Synthesis of the substrate molecules

All reactions were performed under a dry argon atmosphere. Tetrahydrofuran (THF) and Diisopropylamine (DIPA) were degassed under reduced pressure. Iodobenzene, Copper iodide, TMS-acetylene-$^{13}C_2$, TMS-acetylene, TBAF 1M in THF were purchased from Sigma Aldrich, Bis(triphenylphosphine)palladium(II) dichloride was purchased from Acros and 4-iodopyridine was purchased from AK Scientific. All purchased chemicals were used without further purification. Reactions were monitored by TLC on silica gel aluminum-backed plates.

Bis(triphenylphosphine)palladium(II) dichloride (14.4 mg, 0.0206 mmol), copper iodide (8.86 mg, 0.0465 mmol) and 4-iodopyridine (0.15490 g, 0.7178 mmol) were added into a 25 mL glass tube and degassed for 1 h under reduced pressure. Then, THP-DIPA (2:1 v/v, 7 mL) was added to dissolve them and TMS-acetylene-$^{13}C_2$ (107.5 µL, 0.7084 mmol) was slowly added. The mixture was stirred at 50 °C for 24 h. After cooling reaction mixture at room temperature, TBAF 1M in THF (1 mL, 1 mmol) was added and stirred at room temperature for 10 min. Next, iodobenzene(0.4 mL, 3.574 mmol) was added and the mixture was stirred at 50 °C for 26 h. The mixture was concentrated and the residue was isolated by extractive work-up with CH_2Cl_2-brine. The combined organic phase was dried using anhydrous Na_2SO_4 and concentrated. Flash column chromatography was performed using 100 % ethyl acetate and yielded 4-(phenylethynyl-1,2-$^{13}C_2$)pyridine (0.1172 g, 0.6468 mmol, 91.3 %).

Bis(triphenylphosphine)palladium(II) dichloride (8.62 mg, 0.01228 mmol), copper iodide (11.89 mg, 0.0624 mmol) and 4-iodopyridine (0.4032 g, 1.967 mmol) were added into a 10 mL glass tube and degassed for 1 h under reduced pressure. Then, THP-DIPA (4:1 v/v, 4.5 mL) was added to dissolve them and TMS-acetylene-$^{13}C_2$ (110 µL, 0.7124 mmol) was slowly added. The mixture was stirred at 70 °C for 23 h. After cooling reaction mixture at room temperature, TBAF 1M in THF (1mL, 1 mmol) was added and the mixture was stirred at 70 °C for 20 h. Extractive work-up (CH_2Cl_2-brine) was followed by concentration. The combined organic phase was dried using anhydrous Na_2SO_4 and concentrated. Flash column chromatography was performed using

100 % ethyl acetate and yielded 1,2-di(pyridin-4-yl)ethyne-1,2-$^{13}C_2$ (0.1054 g, 0.578 mmol, 81.2 %).

1.2 Polarization of the ^{13}C due to hydrogenation

Though the substrates are relatively stable during the SABRE-SHEATH experiments, after long time of *para*-H_2 bubbling, hydrogenation happens for the acetylenic triple bond and *para*-H_2 induced polarization (PHIP) is observed. In our case, since the *para*-H_2 is bubbled at a low field in the magnetic shield (62 mG), the hydrogenated ^{13}C spin pair will remain in its singlet state until transferred to the magnet for read out. This polarization effect particularly matches the ALTADENA (Adiabatic Longitudinal Transport After Dissociation Engenders Net Alignment) phenomenon, the spectrum is shown below.

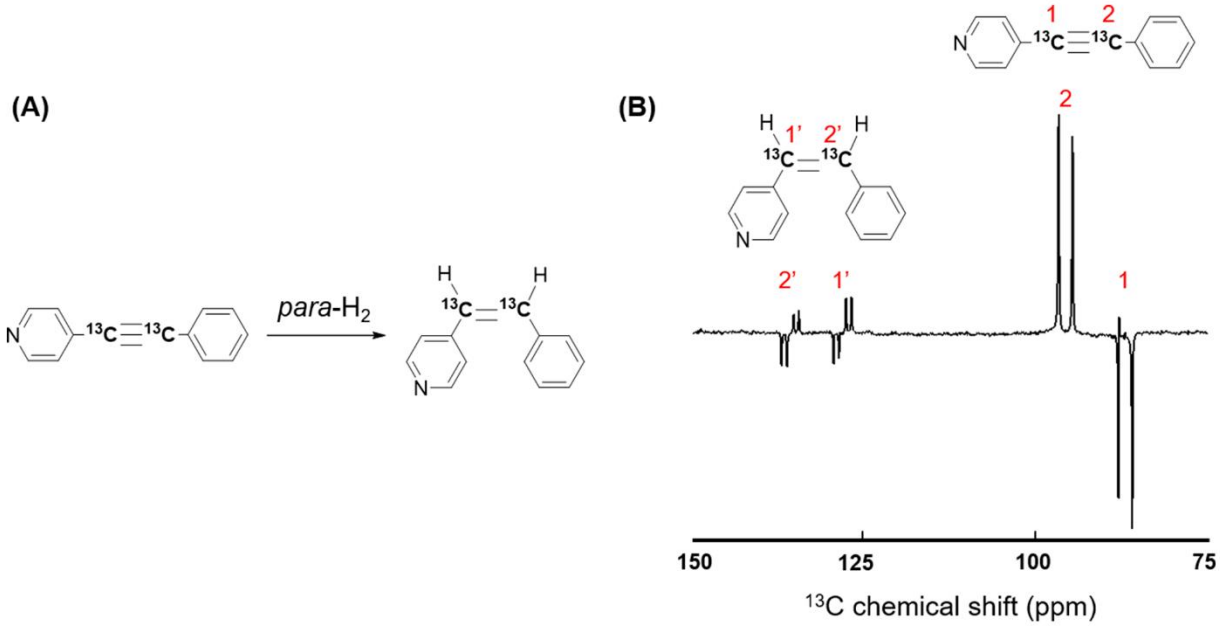

Figure S1. Hydrogenation of the acetylenic triple bond (A) and spectrum of ^{13}C hyperpolarization in the shield at 62 mG (B). On the right part of the spectrum around 90 ppm, is the SABRE hyperpolarized singlet of the original substrate. However, a fraction of the substrate (~10%) is hydrogenated and generates the polarization induced by *para*-H_2 addition. Here the ALTADENA effect is observed at the chemical shift of ^{13}C around 130 ppm.

1.3 Thermal and hyperpolarized ^{1}H spectra including the hydride region

Thermal and hyperpolarized ^{1}H spectra shown in Figure S2. to help determine the polarization transfer complex. We used asymmetric substrate with 13C at natural abundance, bubble *para*-H_2 through the hyperpolarization mixture inside the magnet at 8.45 T. A 45˚ pulse is applied for read out right after stopping the bubbling. The classical PASADENA effect is expected on the hydrides, which is best observed using a 45˚ pulse.

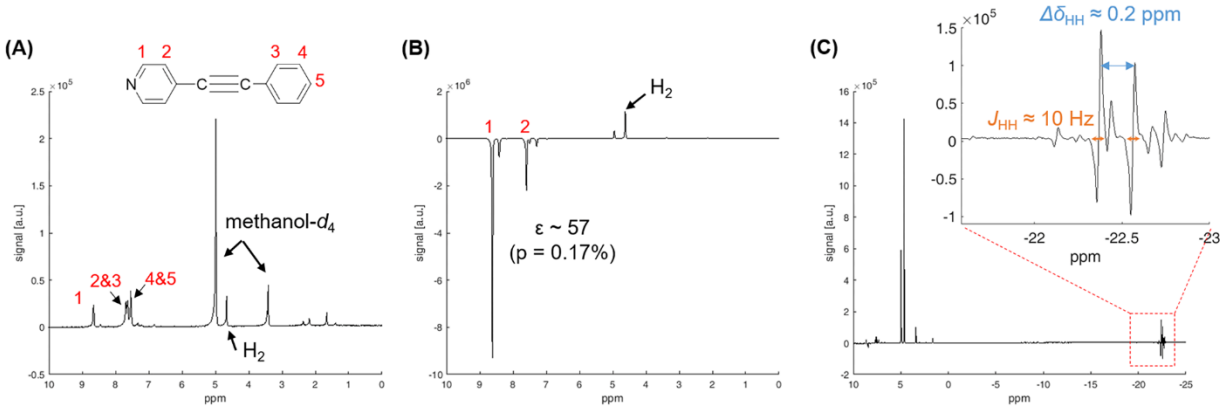

Figure S2. (A) Thermal ^{1}H spectrum of the asymmetric molecule and its peak assignment, note that protons on position 2 and 3 overlap. (Position 3 protons have slightly higher chemical shift than protons in position 2). (B) Hyperpolarized (SABRE) ^{1}H spectrum. *para*-H_2 is bubbled through the sample at 6.5 mT, a ~57 fold enhancement of positions 1 and 2 protons is obtained. However, positions 3, 4 and 5 are not enhanced. (C) Spectrum acquired using 45˚ pulse immediately after stopping bubbling inside the magnet. The hydrides are observed and there are two major resonances with chemical shift difference around 0.2 ppm, as well as clear indications of minor species.

The ^{1}H spectra assist in the structure determination of the PTC species. As shown in Fig. S2 panel B, only the protons on the pyridyl ring are significantly hyperpolarized with enhanced ^{1}H signal. Clearly identifying a strong contribution of the N-binding model. The hydride region shows that in addition to a principle species, additional complexes exist in solution consistent with the fact that we observe SABRE as well as PHIP via hydrogenation. (In section 4 of this SI, we analyze various structures and compare their relative energies.)

1.4 Thermal and hyperpolarized ^{13}C spectra

Thermal and hyperpolarized ^{13}C spectra are analyzed to obtain the important parameters such as the ^{13}C-^{13}C *J*-coupling, J_{CC}. Other *J*-coupling parameters could also be distinguished from the hyperpolarized spectrum.

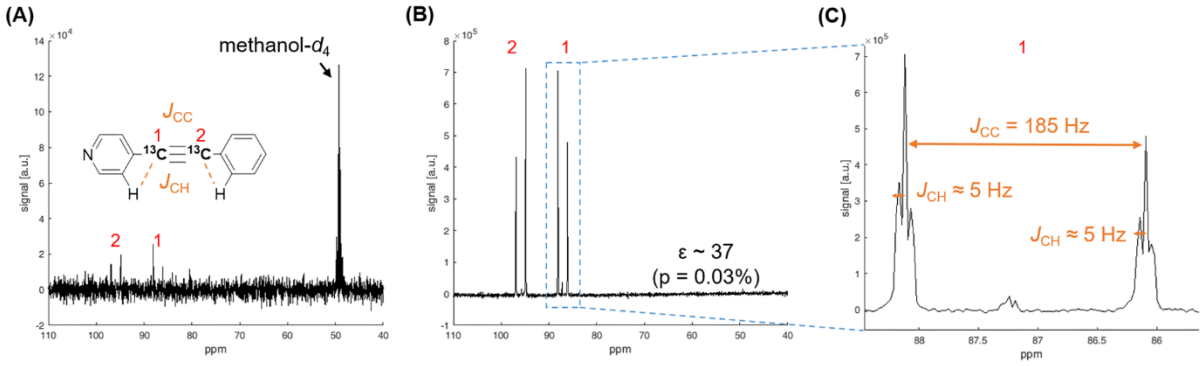

Figure S3. (A) Thermal spectrum of the asymmetric molecule with concentration of 160 mM after one scan. (B) Hyperpolarized ^{13}C spectrum. *para*-H_2 is bubbled through the sample at 0.28 μT, achieving ~37 fold enhancement of the doubly labeled acetylenic carbons. (C) The ^{13}C-^{13}C *J*-coupling, J_{CC}, and the nearby ^{13}C-^{1}H *J*-coupling, could be determined using the hyperpolarized spectrum. The critical parameter

for the polarization transfer, J_{CC}, is 185 Hz; and J_{CH} is around 5 Hz. It is important to point out that by our ab-initio calculations we find J_{CC} values that are very close to this experimental value for the free species and for the N-bound substrate. Whereas, in the substrate bound via C≡C triple bond the J-coupling is reduced to ~120 Hz because of the reduction in triple-bond character upon binding. As indicated in section 3.2 of this SI, this would result in a strong shift in the magnetic field at which SABRE hyperpolarization occurs, which we do not observe leading us to the conclusion that the N-binding species in solution are primarily responsible for the observed SABRE-SHEATH effect.

1.5 Measurements of the lifetime

The magnetization is created in the shield with magnetic field of 0.28 μT, then the sample is positioned at 0.3 mT for relaxation, followed by transport to the magnet for read out. By positioning the sample for different time delays at 0.3 mT, its T_1 lifetime is measured. A similar procedure is used for singlet lifetime measurement. The singlet states are first created in the shield with 6.2 μT then positioned at 0.3 or 50 mT for varying time delays, after which the sample is transferred to the 8.45 T for read out of the antiphase peaks as explained in the main manuscript.

2. Analysis of the polarization transfer

2.1 Derivation of the polarization transfer resonance conditions

First, we consider a four-spin system consisting of two parahydrogen derived hydrides and two ^{13}C spins of the acetylenic bond as depicted in Fig. S2. This represents the direct model, where the substrate is bound to Iridium via the acetylenic bond.

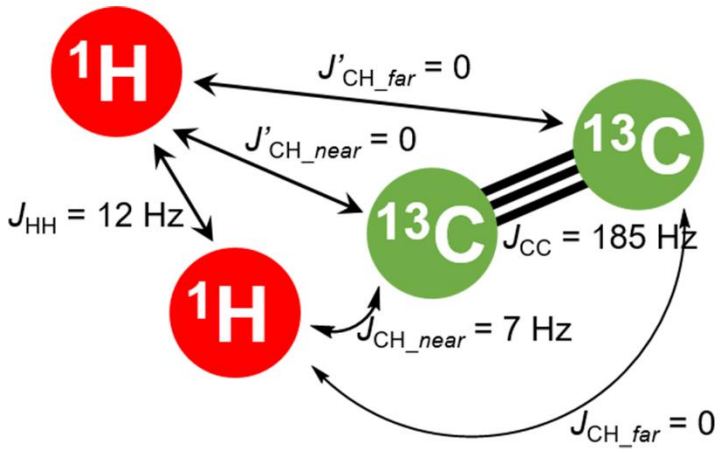

$$\Sigma J_{near} = J_{CH\_near} + J'_{CH\_near}$$
$$\Delta J_{near} = J_{CH\_near} - J'_{CH\_near}$$
$$\Sigma J_{far} = J_{CH\_far} + J'_{CH\_far}$$
$$\Delta J_{far} = J_{CH\_far} - J'_{CH\_far}$$

Figure S4. The 4 spin system of two ^1H and two ^{13}C spins, the iridium metal atom in the middle is omitted. On the left is the rearranging terms for ΔJ_{near} , ΔJ_{far} , ΣJ_{near} and ΣJ_{far} .Approximation of the *J*-coupling values (from both calculation and experimental results) are also shown.

Then its Hamiltonian of this system can be expressed as:

$$H = \nu_H (I_{1Hz} + I_{2Hz}) + \nu_C (I_{1Cz} + I_{2Cz}) + J_{HH} \vec{I}_{1H} \vec{I}_{2H} + J_{CC} \vec{I}_{1C} \vec{I}_{2C} + J_{CH\_near} \vec{I}_{1H} \vec{I}_{1C} + J'_{CH\_near} \vec{I}_{2H} \vec{I}_{1C} + J_{CH\_far} \vec{I}_{1H} \vec{I}_{2C} + J'_{CH\_far} \vec{I}_{2H} \vec{I}_{2C} \quad \text{(S1)}$$

Introducing the CH-*J*-coupling terms (also illustrated in Figure S2), the sum and the difference of the near and far J_{CH} couplings can be written as:

$$\begin{aligned} \Sigma J_{near} &= J_{CH\_near} + J'_{CH\_near} \\ \Delta J_{near} &= J_{CH\_near} - J'_{CH\_near} \\ \Sigma J_{far} &= J_{CH\_far} + J'_{CH\_far} \\ \Delta J_{far} &= J_{CH\_far} - J'_{CH\_far} \end{aligned} \quad \text{(S2)}$$

Using these definitions, the Hamiltonian is rearranged as:

$$\begin{aligned} H = {} & \nu_H (I_{1Hz} + I_{2Hz}) + \nu_C (I_{1Cz} + I_{2Cz}) + J_{HH} \vec{I}_{1H} \vec{I}_{2H} + J_{CC} \vec{I}_{1C} \vec{I}_{2C} \\ & + \frac{\Sigma J_{near}}{2} (\vec{I}_{1H} \vec{I}_{1C} + \vec{I}_{2H} \vec{I}_{1C}) + \frac{\Delta J_{near}}{2} (\vec{I}_{1H} \vec{I}_{1C} - \vec{I}_{2H} \vec{I}_{1C}) \\ & + \frac{\Sigma J_{far}}{2} (\vec{I}_{1H} \vec{I}_{2C} + \vec{I}_{2H} \vec{I}_{2C}) + \frac{\Delta J_{far}}{2} (\vec{I}_{1H} \vec{I}_{2C} - \vec{I}_{2H} \vec{I}_{2C}) \end{aligned} \quad \text{(S3)}$$

To better understand the Hamiltonian, a matrix representation will be more helpful, which requires to expression the Hamiltonian in the basis that containing its eigenvectors. The most adequate basis at hand is the singlet-triplet basis, which is:

$$\begin{aligned} S_0 &= \frac{1}{\sqrt{2}} \left(|\alpha\beta\rangle - |\beta\alpha\rangle \right) \\ T_+ = |\alpha\alpha\rangle,\ T_0 &= \frac{1}{\sqrt{2}} \left(|\alpha\beta\rangle + |\beta\alpha\rangle \right),\ T_- = |\beta\beta\rangle \end{aligned} \quad \text{(S4)}$$

Using this singlet-triplet basis for both the hydride (from *para*-H_2) and the ^{13}C pair, we can identify all possible 16 combinations of ^{1}H and ^{13}C states, which can be sorted in two groups in terms of their symmetry, they are:

10 symmetric states with respect of exchanging H_1 with H_2 and C_1 with C_2:

$$\begin{aligned} & S_0^H S_0^C,\ T_0^H T_0^C \\ & T_+^H T_-^C,\ T_-^H T_+^C \\ & T_+^H T_+^C,\ T_-^H T_-^C \\ & T_0^H T_+^C,\ T_+^H T_0^C \\ & T_0^H T_-^C,\ T_-^H T_0^C \end{aligned}$$

And 6 antisymmetric states with respect of exchanging H_1 with H_2 and C_1 with C_2:

$$S_0^H T_0^C,\ T_0^H S_0^C$$
$$S_0^H T_+^C,\ T_+^H S_0^C$$
$$S_0^H T_-^C,\ T_-^H S_0^C$$

Having represented the Hamiltonian in the matrix form using the singlet-triple basis (the full matrix is listed at the end of this document), we can see that there are no elements in the matrix that connects the groups with different symmetry. However, within the individual groups, the states are connected and the Hamiltonian can drive the hyperpolarization from the hydride singlet (S_0^H) to other states that generate either hyperpolarized ^{13}C-magnetization by affecting population in the T_+^C , T_-^C states, or $^{13}C_2$-signlet by affecting the S_0^C population.

The initial state is the *para*-H_2 derived singlet on the hydride proton pair and all other states are close to 0 population, thus the initial states have the following populations:

$$\begin{gathered} p(S_0^H S_0^C) = p(S_0^H T_+^C) = p(S_0^H T_0^C) = p(S_0^H T_-^C) = 0.25 \\ p(\text{other states}) = 0 \end{gathered} \tag{S5}$$

Choosing subsets of the connected states from the full Hamiltonian, we can see that magnetization and singlet are hyperpolarized in the shield with different magnetic field. For example, the $S_0^H T_-^C$ and $T_-^H T_0^C$ states are connected:

$$\begin{array}{ccc} & \left|S_0^H T_-^C\right\rangle & \left|T_-^H T_0^C\right\rangle \\ \left|S_0^H T_-^C\right\rangle & -\nu_C - J_{HH} & \dfrac{-\Delta J_{far} - \Delta J_{near}}{4} \\ \left|T_-^H T_0^C\right\rangle & \dfrac{-\Delta J_{far} - \Delta J_{near}}{4} & -\nu_H \end{array} \tag{S6}$$

At specific magnetic field when the difference of the diagonal elements is made very small, the off-diagonal element will drive the population transferred from from $S_0^H T_-^C$ to $T_-^H T_0^C$, thus reducing population in T_-^C state of carbon and creating hyperpolarized T_+^C state. The corresponding resonance condition, obtained by demanding the diagonal elements be equal, is

$$\nu_H - \nu_C = J_{HH} \tag{S7}$$

Since the chemical shift frequency $\nu = \gamma B_0$, the magnetic field to match this resonance condition is:

$$B_0 = \frac{\nu_H - \nu_C}{\gamma_H - \gamma_C} = \frac{J_{HH}}{\gamma_H - \gamma_C} \tag{S8}$$

Using $J_{HH} \approx 9$ Hz, $\gamma_H = 42.576$ Hz/μT, $\gamma_C = 10.705$ Hz/μT, we can now estimate the magnetic field would be around 3mG, which matches our experimental results.

In addition, magnetization of the ^{13}C pair could also be polarized at relatively higher field in the shield, for example, the subset matrix is:

$$\begin{array}{c|ccc} & \left|S_0^H S_0^C\right\rangle & \left|T_+^H T_-^C\right\rangle & \left|T_-^H T_+^C\right\rangle \\ \left|S_0^H S_0^C\right\rangle & -(J_{CC}+J_{HH}) & \dfrac{\Delta J_{far}-\Delta J_{near}}{4} & \dfrac{\Delta J_{far}-\Delta J_{near}}{4} \\ \left|T_+^H T_-^C\right\rangle & \dfrac{\Delta J_{far}-\Delta J_{near}}{4} & \nu_H-\nu_C-\dfrac{\Sigma J_{near}+\Sigma J_{far}}{4} & 0 \\ \left|T_-^H T_+^C\right\rangle & \dfrac{\Delta J_{far}-\Delta J_{near}}{4} & 0 & \nu_C-\nu_H+\dfrac{\Sigma J_{near}+\Sigma J_{far}}{4} \end{array} \quad \text{(S9)}$$

Changing the magnetic field by adjusting the current in the coil, once again the diagonal elements could be made equal, and the off-diagonal element will drive the population from $\left|S_0^H S_0^C\right\rangle$ to either $\left|T_+^H T_-^C\right\rangle$ or $\left|T_-^H T_+^C\right\rangle$, polarizing the $\left|T_-^C\right\rangle$ or $\left|T_+^C\right\rangle$ state of the carbons. The corresponding resonance condition is:

$$\nu_H-\nu_C=-(J_{CC}+J_{HH})+\frac{\Sigma J_{near}+\Sigma J_{far}}{4} \quad \text{(S10a)}$$

Or:

$$\nu_H-\nu_C=(J_{CC}+J_{HH})+\frac{\Sigma J_{near}+\Sigma J_{far}}{4} \quad \text{(S10b)}$$

In the spin system, since $\frac{\Sigma J_{near}+\Sigma J_{far}}{4}\approx\frac{7+0}{4}=1.75$ Hz, which is much smaller than the $J_{CC}+J_{HH}\approx 185+9=194$ Hz, the sum of the *J*-coupling term could be dropped and the resonance condition could be simplified as:

$$\nu_H-\nu_C=\pm(J_{CC}+J_{HH}) \quad \text{(S10)}$$

The negative sign corresponds to turning the magnetic field in the shield to the other direction. Also, since now the matching condition is around 194 Hz, which is much larger than the previous condition, using this number and equation S8 again, the magnetic field is around 60 mG, which is also consistent with our experimental results.

On the other hand, we can establish the singlet polarization condition by examining the Hamiltonian matrix subset that connects the hydride singlet and singlet on carbons, one example is:

$$\begin{array}{ccc} & S_0^H T_+^C & T_+^H S_0^C \\ S_0^H T_+^C & -J_{HH}+\nu_C & \frac{\Delta J_{near}-\Delta J_{far}}{4} \\ T_+^H S_0^C & \frac{\Delta J_{near}-\Delta J_{far}}{4} & -J_{CC}+\nu_H \end{array} \quad \text{(S11)}$$

And the resonance condition to polarize S_0^C state on carbon is:

$$\nu_H - \nu_C = J_{CC} - J_{HH} \quad \text{(S12)}$$

Accordingly, that is a 176 Hz difference and the matching magnetic field would be around 50 mG, which is similar to the second magnetization polarization condition and matches with experiments.

As discussed in the article, the direct binding model may only have a small contribution to the observed SABRE spectra and we conclude that the hyperpolarization transfer is more likely through a larger spin system of additional protons in the pyridine rings. In this case, iridium of the catalyst binds with the nitrogen of the pyridyl ring, thus forming an eight-spin system (2 *para*-H_2 protons, 4 pyridyl protons and 2 carbon-13s); In the following section we find by numerical simulation that the general behavior of the two models is surprisingly similar. At the end, we can use the relative positions of the resonances to distinguish the two models as described in the following.

2.2 Spin dynamics of low to high field sample transfer

Hyperpolarization of both magnetization and singlet order, which are generated at low field, are detected in the 8.45 T high field inside the magnet. The transfer process of the sample is highly adiabatic, indicating that the population will stay at eigenstates of the system during transfer.

Since magnetization is represented as $I_{1z}+I_{2z}$, which is associated with population difference between the $\alpha\alpha$ and $\beta\beta$ states, they are eigenstates at both low and high fields. Therefore magnetization remains unchanged during the transfer process. When a 90˚ pulse is applied in the magnet, we will obtain an in-phase spectrum, as shown in the main article in Figure 3B(1).

The singlet order, however, is only an eigenstate at low magnetic field and is not detectable. It is converted into a detectable state during transfer from low to high field if a chemical shift difference between the two ^{13}C spins exists. To enable this transformation, we designed the asymmetric molecule 1-phenyl-2-(4-pyridyl) acetylene, with the chemical shift difference of the two acetylenic ^{13}C spins of 9 ppm. At low magnetic field, e.g. 100 G and below, the chemical shift difference ($\Delta\delta \leq 1$ Hz) is much smaller than their *J*-coupling (J_{CC} =185 Hz), so the system is strongly coupled and the singlet order is eigenstate, that is well protected from coherent evolution and subsequent relaxation.

The singlet will not be an eigenstate at high magnetic fields. We calculated the associated eigenstate as function of magnetic field, (or rather, the frequency difference between the ^{13}C spins, $\Delta\nu$, which is proportional the magnetic field):

$$\left|eigenstate(\Delta\nu)\right\rangle = \frac{\sqrt{\Delta\nu^2 + J_{CC}^2} - \Delta\nu}{J_{CC}}\left|\alpha\beta\right\rangle - \left|\beta\alpha\right\rangle \tag{S13}$$

Accordingly, the field dependent density matrix is:

$$\rho(\Delta\nu) = \left|eigenstate(\Delta\nu)\right\rangle\left\langle eigenstate(\Delta\nu)\right| \tag{S14}$$

The initial density matrix of the singlet when Δν = 0 is:

$$\rho_0 = \frac{1}{4}\hat{\mathbf{1}} - (I_{1z}I_{2z} + I_{1x}I_{2x} + I_{1y}I_{2y}) \tag{S15}$$

By raising the magnet field this density matrix becomes:

$$\rho(\Delta\nu) = \frac{1}{4}\hat{\mathbf{1}} - I_{1z}I_{2z} - \frac{J_{CC}}{\sqrt{\Delta\nu^2 + J_{CC}^2}}(I_{1x}I_{2x} + I_{1y}I_{2y}) - \frac{\Delta\nu}{\sqrt{\Delta\nu^2 + J_{CC}^2}}\frac{1}{2}(I_{1z} - I_{2z}) \tag{S16}$$

When $\rho(\Delta\nu)$ is probed with a 90˚ pulse at 8.45 T (Δν = 815 Hz), only the I_{1z}-I_{2z} component yields signal in two anti-phase doublets, and plugging in the numbers we would have 98% singlet detected, compared with a infinite high detection magnetic field case (where Δν = ∞ and the density matrix corresponds to $\rho(\Delta\nu) = \frac{1}{4}\hat{\mathbf{1}} - I_{1z}I_{2z} - \frac{1}{2}(I_{1z} - I_{2z})$, which is a pure population of the $\beta\alpha$ state).

3. Numerical simulation

3.1 Full range simulation of the 4 spin system

To better illustrate the mechanism of the polarization transfer, we used the Matlab package, Spinach, to simulate the magnetization and singlet polarization of ^{13}C as a function of the magnetic field. The full range simulation from negative to positive magnetic field, as well as all the resonance conditions are shown below.

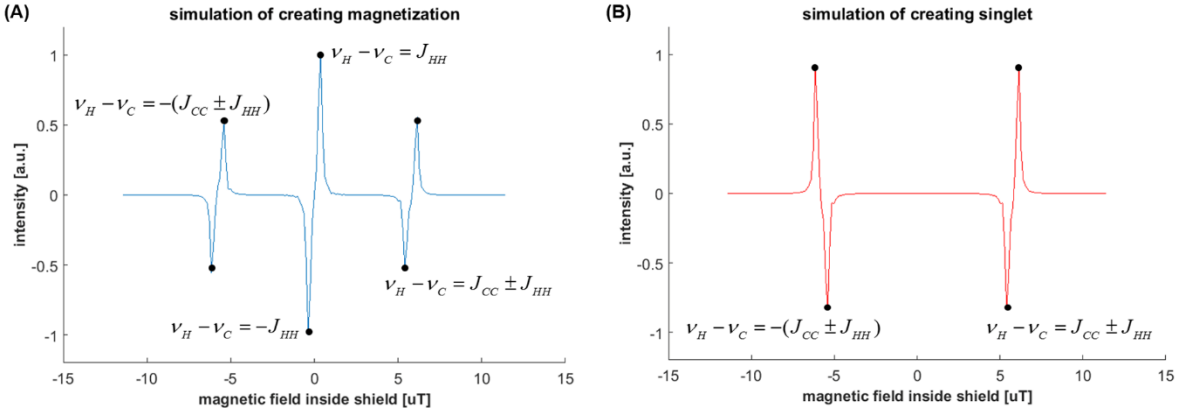

Figure S5. Simulation of the polarization transfer of magnetization (A) and singlet (B), with the magnetic field ranging from -12 to 12 μT. Highlighted points are all the resonance conditions where the polarization transfer is maximized.

For the magnetization simulation, the low field polarization around 0.3 μT matches well with the experiment and our derivation. However, at around 6 μT, there is splitting between the magnetization polarizations of about $2J_{HH}$. The experimental magnetization data also indicates that behavior, however not as clearly as the simulations. We believe that magnetization can be strongly affected by the sample transfer from inside the shield to the magnet. Specifically, crossing strong magnetic field gradients or magnetic field inversion points may cause non-adiabatic evolution of the magnetization, which causes broader features in the experiment.

The singlet simulation shows great consistency with our experiment. There is no singlet polarized at extremely low field. The singlet is only polarized at around 6 μT, and the splitting of around $2J_{HH}$ is clearly observed in the experiment, which could be due to the immunity of singlet to magnetic fields. Furthermore, the polarization level of the singlet is quite high at 6 μT, indicating that polarization of the singlet is efficient; this is also consistent with the experimental results.

3.2 Comparison between the simulation of direct and indirect polarization transfer

Since the nature of the binding mode in the real system was in question, we use simulation to detect if there are differences of the polarization transfer transitions between the two modes. We simulate the direct and indirect model and vary parameter of the *J*-coupling terms used in the simulation. As illustrated in Fig. S6, we find that the direct and indirect polarization transfer spin systems tend to give quite similar transfer patterns for comparable *J*-coupling constants in the source (J_{HH}) and the final target (J_{CC}).

As apparent from Fig. S6 in combination with the analytical expressions provided in the main manuscript for the resonance conditions, the polarization profile is determined by two critical *J*-coupling parameters, J_{HH} and J_{CC}. J_{HH} determines the position of the first resonance condition for forming magnetization. J_{HH} also controls the distance between the two resonance conditions at higher fields. Finally, J_{CC} dictates the overall position of the higher field resonances. This is true irrespective of the hyperpolarization transfer pathway (direct or indirect).

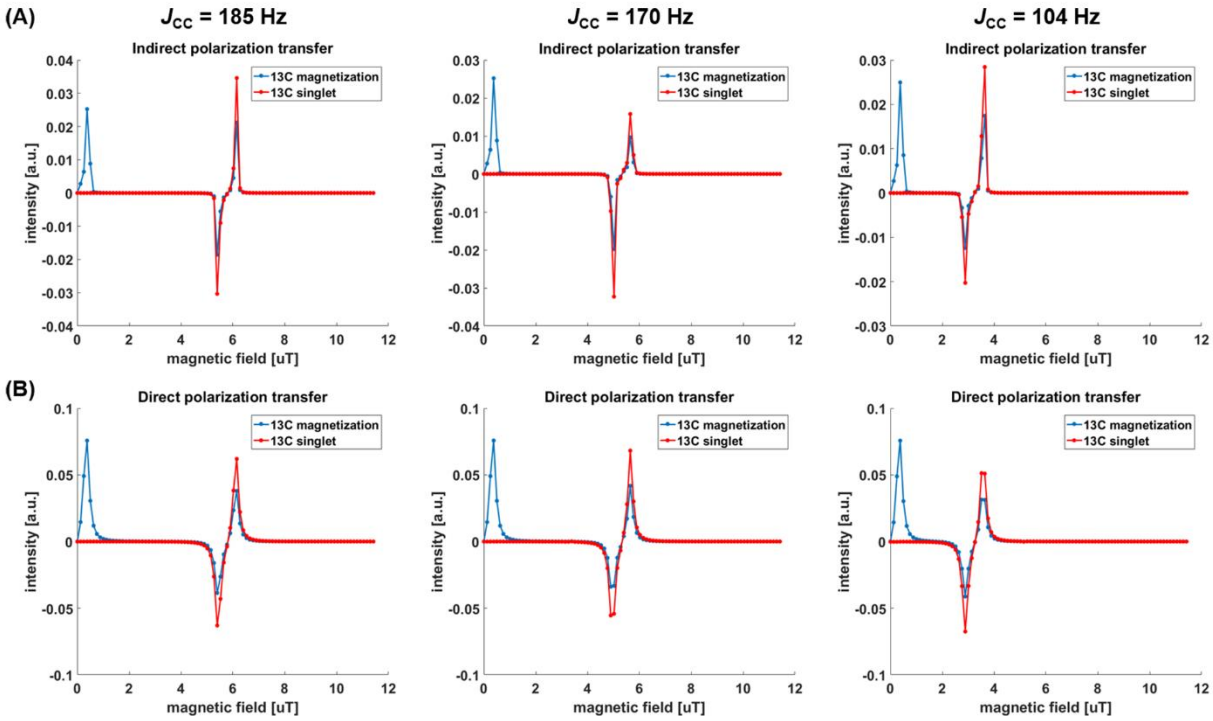

Figure S6. Matlab simulation using the Spinach package, for the indirect polarization transfer (A, where there are 8 spins in the system) and the direct polarization transfer (B, where there are 4 spins in the system). Simulation shows similar pattern of the magnetization and singlet for indirect or direct polarization transfer. On the other hand, the magnetic field position at which the singlet peak appears is closely related with the J_{CC} coupling: the stronger this coupling is, the further away the singlet peak will appear.

3.3 Simulation at the optimal ^{1}H hyperpolarization field (6.5 mT)

In addition to the simulation of the polarization transfer at low field (from -12 to 12 6 μT), simulations at higher field (6.5 mT) where ^{1}H hyperpolarization works best are also performed. However, all of the simulations give 0 transfer to ^{13}C, which is as expected because at such field there is no energy level crossing between ^{1}H and ^{13}C spins. Although polarization transferred to ^{1}H, there is still no energy level crossing between the auxiliary ^{1}H's and ^{13}C's. This is also consistent with the experimental results, the ^{13}C hyperpolarization is negligible when bubbling at 6.5 mT.

4. DFT calculation of PTC complexes.

In addition to the spin dynamics simulations, the binding mode was also investigated with DFT calculations using the all-electron FHI-aims code[1]. The *tight* settings were used for the integration grids and basis sets. We used the PBE exchange-correlation functional[2] plus Tkatchenko-Scheffler vdW correction[3]. In Fig. S8, the total energy of each configuration is taken as a sum of its isolated components (e.g., separate calculations were performed for Cl^{-}, H_2, etc.). In the article we showed two major binding complexes. Here we displayed the full process of

catalyst activation and energy differences of all possible PTC's. The geometries were first built by hand and minimized in Jmol and then relaxed with FHI-aims. No extensive conformational search was performed. The geometries are shown in Table S2. Here we compare the ground state energies only and do not consider other energy contributions (vibrations, solvent effects, …). We conclude that the indirect transfer should be the main polarization process. In case the acetylenic bond is complexed to the Iridium, the calculated C-C *J*-coupling is only 120 Hz, whereas for the substrate bound via nitrogen, J_{CC} is calculated to be on the order of 191 Hz, more in line with the experimental data. The *J*-couplings were calculated nonrelativistically with FHI-aims. Table S1 presents a basis set convergence study for the *J*-coupling of the PTC of Fig. 2A. We have taken the Dunning cc-pVnZ basis sets[4] and uncontracted all the s-functions, which we denote u-cc-pVnZ. Uncontraction is necessary since it gives the basis sets extra flexibility in the core region, which is necessary to converge the difficult Fermi contact (FC) contribution of the *J*-coupling.[5] Using the regular contracted cc-pVnZ basis sets would lead to poor convergence of FC and therefore the total *J*-coupling. After doing a convergence study with the u-cc-pVnZ for the PTC of Fig. 2A, we used a fully uncontracted cc-pV5Z to calculate the final *J*-couplings for both PTC. Using u-cc-pV5Z we estimate the basis set error to be within a few percent.

Table S1. Basis set convergence study for the PTC of Fig. 2A. u-cc-pVnZ refers to the regular cc-pVnZ basis sets with the s functions uncontracted. A fully uncontracted cc-pV5Z basis set yields 190.7 Hz, showing that the dominant contribution to the *J*-couplings comes from the core s orbitals.

u-cc-pVDZ	176.8 Hz
u-cc-pVTZ	179.3 Hz
u-cc-pVQZ	187.0 Hz
u-cc-pV5Z	190.8 Hz

Activation

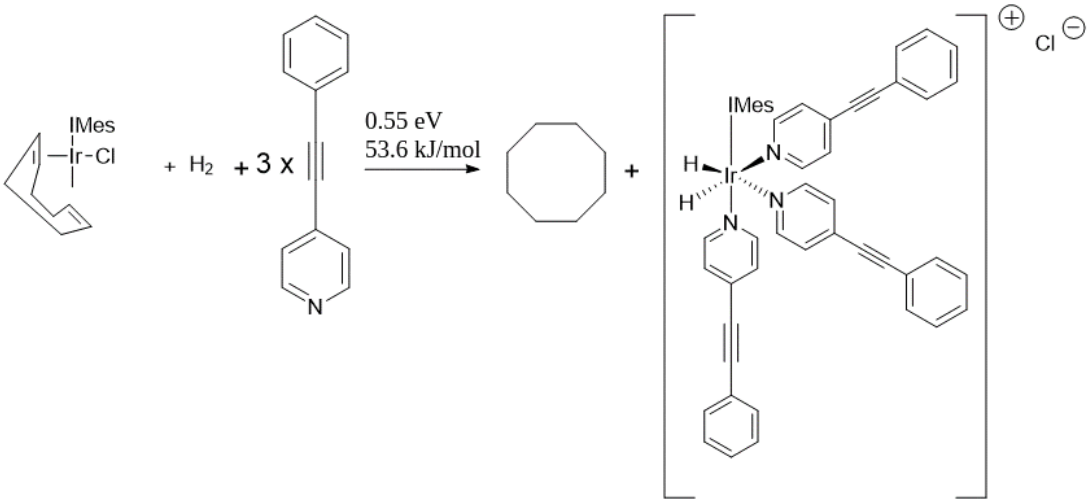

Equilibria and Energies of interest:

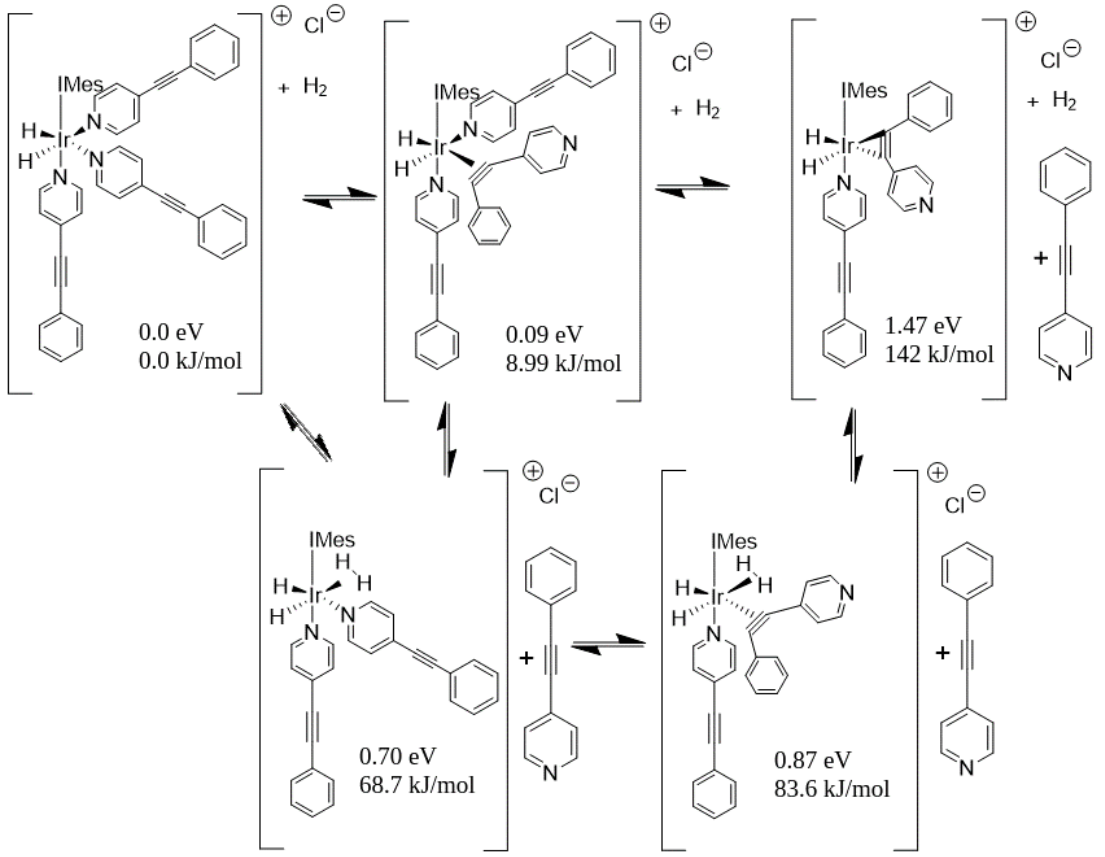

Figure S8. DFT calculation of the activation process and equilibria and energies of interest. During activation, the COD (cyclooctadiene) will disassociate from the iridium core, then H_2 and the substrate will bind with the iridium, either with three N or the ^{13}C triple bond.

Table S2. Geometries of the configuration as shown in Fig. S5 in the format of FHI-aims geometry files.

PTC 1 – 0.0 eV:

atom 13.11576225 4.94961535 7.18532949 C
atom 10.90718940 5.47963132 6.85291789 C
atom 11.47867245 6.52825957 7.49109625 C
atom 13.73656820 7.13837865 8.26564473 C
atom 14.41196785 8.02519222 7.41016670 C
atom 15.28193896 8.95307567 7.98311527 C
atom 15.47771165 9.02469659 9.36751890 C
atom 14.76147947 8.14515954 10.18374824 C
atom 13.87871018 7.19330295 9.65882410 C
atom 14.19776584 7.98473277 5.92222996 C
atom 14.24930779 6.95811679 5.53669221 H
atom 14.95020238 8.58894345 5.40340215 H
atom 13.20584477 8.37443915 5.64943669 H
atom 16.44951408 10.01544547 9.94878491 C
atom 17.46306466 9.85240963 9.55327997 H
atom 16.49435821 9.94318002 11.04180964 H
atom 16.16969660 11.04646569 9.69063548 H
atom 13.10904365 6.26970502 10.56161419 C
atom 12.02561003 6.44137593 10.48541652 H
atom 13.39811557 6.41838943 11.60800079 H
atom 13.28581529 5.21809630 10.29678203 H
atom 11.67568783 3.32767005 5.90964002 C
atom 11.40460462 2.12517189 6.57955236 C
atom 11.28029114 0.96645168 5.80449083 C
atom 11.37664748 0.99009336 4.41018012 C
atom 11.54856933 2.22673153 3.78020939 C

atom	11.68908387	3.41072433	4.50650871	C
atom	11.19350971	2.08110944	8.06831118	C
atom	12.01192681	2.56369192	8.61634427	H
atom	11.10673072	1.04571190	8.41674333	H
atom	10.26511343	2.60415039	8.34254830	H
atom	11.28763047	-0.27243964	3.59636759	C
atom	10.40839546	-0.26094057	2.93662754	H
atom	11.21639643	-1.16107249	4.23443107	H
atom	12.16935925	-0.38553156	2.94848281	H
atom	11.79750749	4.73018374	3.78961395	C
atom	10.81918011	5.23248131	3.75122691	H
atom	12.13090905	4.58438764	2.75596623	H
atom	12.48764385	5.42493518	4.28275111	H
atom	16.95811952	5.99229109	6.29031123	C
atom	17.98024545	6.92497578	6.34177254	C
atom	18.46842923	7.35540373	7.59179129	C
atom	17.89096363	6.75629235	8.72910975	C
atom	16.86627071	5.84058229	8.58125159	C
atom	14.93389243	1.82651014	5.14176875	C
atom	14.91551377	1.24189173	3.89027166	C
atom	14.90897423	2.05079145	2.73520301	C
atom	14.95176730	3.44360981	2.94561313	C
atom	14.96206111	3.94123496	4.23704649	C
atom	16.30377590	1.79933763	9.04368020	C
atom	17.31615797	0.94878141	9.44500898	C
atom	18.51276774	0.87012459	8.69927659	C
atom	18.59222207	1.68966833	7.55461605	C
atom	17.53182749	2.51318319	7.22079698	C

atom	14.78760665	3.87659582	7.42070051	Ir
atom	14.60858277	4.21550582	8.96247465	H
atom	13.79560641	2.66926846	7.62093925	H
atom	16.36717449	5.45894172	7.38164240	N
atom	14.94912183	3.16701654	5.34394014	N
atom	16.38737450	2.58889230	7.94293289	N
atom	12.81453293	6.20219498	7.68431021	N
atom	11.90142723	4.53070682	6.66395394	N
atom	9.89418198	5.31698638	6.51059995	H
atom	11.07089240	7.47246738	7.82609062	H
atom	11.58926603	2.27161782	2.69022347	H
atom	11.09481601	0.01753499	6.31098530	H
atom	15.82986061	9.63406119	7.32932181	H
atom	14.89135110	8.19578464	11.26633671	H
atom	14.82203317	1.49247192	1.44488593	C
atom	14.59229049	0.42063372	-0.95256762	C
atom	14.52163586	-0.98109332	-1.10178607	C
atom	14.39624795	-1.54295173	-2.36751520	C
atom	14.33945345	-0.72402847	-3.49875070	C
atom	14.40912916	0.66514280	-3.36132348	C
atom	14.53467885	1.23892698	-2.10095175	C
atom	14.93524934	5.01600160	4.40650229	H
atom	14.94552207	4.12913432	2.10074609	H
atom	14.90337849	1.21543978	6.04069680	H
atom	14.87811532	0.15829841	3.80228655	H
atom	14.71658881	0.99718304	0.33349706	C
atom	14.59026484	2.32042353	-1.98613174	H
atom	14.24128021	-1.16890500	-4.48840612	H

atom 14.36551022 1.30344860 -4.24314454 H

atom 14.56779066 -1.61276333 -0.21585924 H

atom 14.34278249 -2.62583486 -2.47457130 H

atom 19.46123099 8.34876397 7.70725824 C

#magnetic_response

atom 20.29829876 9.22970430 7.82834190 C

#magnetic_response

atom 21.26462681 10.25298674 7.97397694 C

atom 21.67740689 10.66490635 9.25928735 C

atom 22.62447716 11.67347278 9.39864814 C

atom 23.17333686 12.28468615 8.26786776 C

atom 21.82491638 10.87604062 6.83848026 C

atom 22.77147643 11.88324688 6.99080452 C

atom 19.56805485 0.01920746 9.08048118 C

atom 20.48074501 -0.71872793 9.41816032 C

atom 21.53683251 -1.57355742 9.81208383 C

atom 21.41260125 -2.37513308 10.96721003 C

atom 22.45395340 -3.21290233 11.35069034 C

atom 23.62889782 -3.26646296 10.59553817 C

atom 23.76140099 -2.47663601 9.44999682 C

atom 22.72715020 -1.63483743 9.05615344 C

atom 22.82297921 -1.01629766 8.16504164 H

atom 24.44212494 -3.92445254 10.90009173 H

atom 24.67728476 -2.51846488 8.86144919 H

atom 20.49420771 -2.32776452 11.55042646 H

atom 22.35061734 -3.82853529 12.24359171 H

atom 15.37606197 1.87734315 9.60476810 H

atom 17.18639962 0.34290464 10.33918630 H

atom	19.48378205	1.67942524	6.93126700	H
atom	17.58342333	3.14781127	6.33868523	H
atom	16.58353244	5.65743937	5.32595868	H
atom	18.39417299	7.32780198	5.41959766	H
atom	18.22578748	7.03337947	9.72618201	H
atom	16.38773286	5.39371278	9.44866032	H
atom	21.50729609	10.55764463	5.84670330	H
atom	23.91539528	13.07419038	8.38197572	H
atom	23.19987151	12.35919509	6.10937507	H
atom	21.24651038	10.18270892	10.13557218	H
atom	22.93829256	11.98560693	10.39416959	H

PTC 2 – 0.09 eV:

atom	12.61994096	4.68725628	7.21135120	C
atom	10.39359377	4.97555886	6.74583996	C
atom	10.78144088	6.01607156	7.51784122	C
atom	12.83583669	6.81681346	8.57386436	C
atom	13.44288772	7.88917444	7.90028382	C
atom	14.05440229	8.87552444	8.67437741	C
atom	14.05243718	8.82495592	10.07527131	C
atom	13.40424405	7.75899460	10.69996801	C
atom	12.78026552	6.74093539	9.97102203	C
atom	13.40868356	7.97821802	6.39979965	C
atom	13.83947757	7.08123482	5.93456690	H
atom	13.97364496	8.84637643	6.04428548	H
atom	12.37805455	8.07080900	6.02712158	H
atom	14.74133759	9.89269743	10.87904577	C
atom	15.81377106	9.93331279	10.64062641	H
atom	14.64531327	9.70981898	11.95529194	H

atom	14.32473420	10.88659030	10.66330188	H
atom	12.06440256	5.62019575	10.67196358	C
atom	10.97281770	5.75088889	10.62302095	H
atom	12.34865838	5.58321848	11.72924630	H
atom	12.29198044	4.64629636	10.22009118	H
atom	11.44275568	2.99647050	5.73587139	C
atom	11.29025601	1.73241155	6.32274907	C
atom	11.29126795	0.61844294	5.47207251	C
atom	11.39484656	0.74071615	4.08597318	C
atom	11.44960872	2.02804136	3.53833210	C
atom	11.46457958	3.16985416	4.33838210	C
atom	11.06202760	1.54001401	7.79870911	C
atom	11.21278879	2.45788421	8.37368247	H
atom	11.73214306	0.77225863	8.20741301	H
atom	10.03211638	1.19519763	7.97343446	H
atom	11.44417092	-0.46755896	3.19149448	C
atom	10.61016363	-0.46897796	2.47582443	H
atom	11.39695628	-1.39987635	3.76612068	H
atom	12.37084801	-0.47764060	2.59837175	H
atom	11.45724353	4.53596677	3.70555022	C
atom	10.43489380	4.94104374	3.66543324	H
atom	11.82868829	4.48770018	2.67578648	H
atom	12.06274633	5.26421815	4.25835295	H
atom	17.63244084	8.13245116	5.36910657	C
atom	16.84648593	7.49634177	6.32435644	C
atom	16.62623581	6.10580573	6.23062265	C
atom	17.24615017	5.45023699	5.14864348	C
atom	18.02076134	6.18377482	4.25307197	C

atom	14.76027853	1.80395007	5.13793564	C
atom	14.86773688	1.30923958	3.85295780	C
atom	14.83973729	2.19378537	2.75453726	C
atom	14.72602067	3.56607058	3.05352005	C
atom	14.61577488	3.97562390	4.36976072	C
atom	15.81162127	1.41741426	8.89350795	C
atom	16.80971245	0.55620968	9.30635633	C
atom	18.13462461	0.74217473	8.85357451	C
atom	18.35325099	1.83222979	7.98701248	C
atom	17.29734466	2.65194180	7.62837824	C
atom	14.38491987	3.74329567	7.50418597	Ir
atom	13.90305922	3.71752652	9.01248981	H
atom	13.45070663	2.45250015	7.60140425	H
atom	18.21854661	7.50660444	4.33617228	N
atom	14.62951274	3.12176764	5.41645769	N
atom	16.02948900	2.46418951	8.05913466	N
atom	12.13001959	5.83584502	7.79189773	N
atom	11.50911096	4.17323549	6.56135053	N
atom	9.43706758	4.72430033	6.30840570	H
atom	10.23854743	6.86967233	7.90044482	H
atom	11.49633680	2.14658441	2.45425491	H
atom	11.19617266	-0.37515247	5.91453667	H
atom	14.53368090	9.71740958	8.17031532	H
atom	13.39861891	7.70134806	11.78913432	H
atom	14.88885620	1.72249774	1.42888085	C
atom	14.92848966	0.82387972	-1.04856666	C
atom	14.99523747	-0.56275138	-1.30386690	C
atom	15.01425955	-1.03038315	-2.61300770	C

atom	14.96799891	-0.13095562	-3.68200320	C
atom	14.90244623	1.24400961	-3.43919109	C
atom	14.88234483	1.72423777	-2.13461893	C
atom	14.50725529	5.02876321	4.61381451	H
atom	14.70687403	4.30620835	2.25669847	H
atom	14.75490597	1.13328011	5.99330607	H
atom	14.95095031	0.23656974	3.69392474	H
atom	14.90740509	1.30557787	0.28093844	C
atom	14.83302476	2.79396270	-1.93694604	H
atom	14.98402611	-0.50218937	-4.70615733	H
atom	14.86778800	1.94430080	-4.27295435	H
atom	15.03327243	-1.25668545	-0.46542535	H
atom	15.06658734	-2.10178030	-2.80324937	H
atom	15.84102448	5.42795795	7.22356969	C
atom	15.55428896	5.28587256	8.46018865	C
atom	15.88855562	5.59615530	9.82563466	C
atom	15.46181285	4.82346256	10.91827859	C
atom	15.80884505	5.17683777	12.21893868	C
atom	16.59862856	6.30380250	12.45512339	C
atom	16.70168147	6.72206773	10.07612374	C
atom	17.05150811	7.06769593	11.37593733	C
atom	19.17908627	-0.11361373	9.25048672	C
atom	20.08560853	-0.85371739	9.60017671	C
atom	21.13561007	-1.70925791	10.00662267	C
atom	20.88030445	-2.78473960	10.88448530	C
atom	21.91716626	-3.62125382	11.28198087	C
atom	23.21629921	-3.40218079	10.81493036	C
atom	23.47894265	-2.33984396	9.94526661	C

atom	22.45078164	-1.49608994	9.54044734	C
atom	22.64697922	-0.66560480	8.86401105	H
atom	24.02557811	-4.06025754	11.12962808	H
atom	24.49187215	-2.16947614	9.58226372	H
atom	19.86554912	-2.94788704	11.24429326	H
atom	21.71347394	-4.44914709	11.96017749	H
atom	14.78598344	1.28842303	9.22998770	H
atom	16.56988543	-0.26145741	9.98251333	H
atom	19.34943016	2.03908604	7.60203564	H
atom	17.46059423	3.50880253	6.98107374	H
atom	17.80441723	9.20974545	5.43521092	H
atom	16.39471803	8.06578446	7.13453260	H
atom	17.13861531	4.37668390	5.00846607	H
atom	18.51015561	5.67749052	3.41711158	H
atom	17.04587578	7.32743164	9.23998082	H
atom	16.86777589	6.58119529	13.47381825	H
atom	17.67711122	7.94265923	11.55114704	H
atom	14.84575323	3.94458950	10.73635414	H
atom	15.46345426	4.56794575	13.05427574	H

PTC 3 – 1.47 eV:

atom	12.35633315	4.12024117	8.90819667	C
atom	10.14517555	4.37682646	8.43677494	C
atom	10.56868293	5.51157837	9.04960099	C
atom	12.76029647	6.38398803	9.86811730	C
atom	13.23549059	7.37137230	8.98809280	C
atom	14.04863515	8.37336650	9.51739823	C
atom	14.39467751	8.40625816	10.87277780	C
atom	13.88535560	7.41253915	11.71357623	C

atom	13.04970207	6.39428988	11.24040221	C
atom	12.88119302	7.36037705	7.52607807	C
atom	13.04042342	6.37164468	7.07521612	H
atom	13.49138361	8.08593807	6.97803360	H
atom	11.82489760	7.61960320	7.36318588	H
atom	15.27910108	9.49881555	11.40756157	C
atom	16.12612697	9.68911248	10.73477918	H
atom	15.67548130	9.25052517	12.39923092	H
atom	14.72373981	10.44372822	11.50016445	H
atom	12.46577666	5.37412180	12.17976719	C
atom	11.37069521	5.33337567	12.09605662	H
atom	12.71459979	5.61944464	13.21801281	H
atom	12.83857536	4.36213479	11.97011879	H
atom	11.31630284	2.27817966	7.66471106	C
atom	11.23182910	1.07250186	8.38335317	C
atom	11.34553722	-0.12068298	7.65566532	C
atom	11.48358747	-0.13570715	6.26654492	C
atom	11.51897362	1.09025753	5.58808534	C
atom	11.44559288	2.30743793	6.26027766	C
atom	10.93386607	1.02331306	9.85902430	C
atom	11.04852612	1.99456483	10.34810756	H
atom	11.58753645	0.30596372	10.37180835	H
atom	9.89984190	0.68422544	10.01897579	H
atom	11.56471082	-1.42933878	5.50463823	C
atom	10.56660276	-1.73717785	5.15844460	H
atom	11.95840483	-2.24231716	6.12686322	H
atom	12.19949304	-1.33130384	4.61513003	H
atom	11.50629063	3.60733996	5.50671783	C

atom	10.54950705	4.14717052	5.54819748	H
atom	11.74458474	3.42873588	4.45314863	H
atom	12.26931696	4.28066551	5.92118017	H
atom	14.73809992	1.80385368	3.70875348	C
atom	14.78381356	2.77873301	4.70106719	C
atom	14.84209114	2.37606845	6.04870992	C
atom	14.86260474	0.99420525	6.30666412	C
atom	14.83185791	0.10786823	5.23448744	C
atom	15.44649081	0.64211332	10.20635726	C
atom	16.41440604	-0.31199156	10.45077032	C
atom	17.74946615	-0.08037658	10.05017142	C
atom	18.00840486	1.15162605	9.41157876	C
atom	16.97883625	2.04755009	9.19171269	C
atom	14.05389040	3.12737372	9.15012629	Ir
atom	14.75690559	0.48374955	3.95068921	N
atom	15.69805359	1.81513086	9.56980490	N
atom	11.92235695	5.34690574	9.32828722	N
atom	11.24779535	3.53825476	8.35484767	N
atom	9.17408900	4.08879463	8.05699444	H
atom	10.04195578	6.41825572	9.31497651	H
atom	11.63686460	1.09538007	4.50370899	H
atom	11.29315573	-1.06734744	8.19717410	H
atom	14.44131746	9.13779775	8.84545961	H
atom	14.13067112	7.43437974	12.77677745	H
atom	14.87962388	3.35266334	7.09490305	C
atom	15.25500643	4.38037908	7.72190176	C
atom	15.97643829	5.59452287	7.95454611	C
atom	16.52946872	5.90772866	9.21096001	C

atom	17.28018910	7.06578782	9.37973811	C
atom	17.47923976	7.93797720	8.30801182	C
atom	16.18365823	6.48167843	6.87700244	C
atom	16.92593012	7.64306960	7.05839204	C
atom	18.76371129	-1.02628218	10.27908551	C
atom	19.64129012	-1.85371196	10.47475461	C
atom	20.65523416	-2.81194375	10.69953318	C
atom	20.35231001	-4.03330339	11.33985169	C
atom	21.35370819	-4.97254511	11.55689502	C
atom	22.66336710	-4.71261266	11.14277571	C
atom	22.97294850	-3.50614232	10.50808360	C
atom	21.98085714	-2.55841672	10.28509205	C
atom	22.21285401	-1.61606873	9.79129012	H
atom	23.44467900	-5.45210617	11.31513373	H
atom	23.99406006	-3.30536487	10.18606473	H
atom	19.32949513	-4.22720275	11.65919677	H
atom	21.11427349	-5.91331680	12.05119724	H
atom	14.41652540	0.48828508	10.52286661	H
atom	16.14530777	-1.23549947	10.95860617	H
atom	19.01563898	1.39926473	9.08380807	H
atom	17.16663775	2.98868785	8.68044267	H
atom	14.68251281	2.09777682	2.65793746	H
atom	14.76095533	3.83618972	4.44229573	H
atom	14.89886932	0.61260107	7.32442715	H
atom	14.85376424	-0.96862780	5.41922165	H
atom	15.75219535	6.24723539	5.90474321	H
atom	18.06469790	8.84676437	8.44390222	H
atom	17.07923284	8.32097115	6.21921467	H

atom	16.36681725	5.23642175	10.05280681	H
atom	17.70376579	7.29412723	10.35696626	H
atom	13.38778662	2.62388016	10.52025122	H
atom	14.54383564	4.23349788	10.10570577	H

PTC 4 – 0.70 eV:

atom	12.80623943	4.96547676	7.28498423	C
atom	10.64235778	5.53336666	6.81866377	C
atom	11.16328628	6.52756530	7.57735259	C
atom	13.35919616	7.01511105	8.61689666	C
atom	14.15522515	7.94713822	7.93404468	C
atom	15.01459989	8.74722824	8.69336514	C
atom	15.07961099	8.64729927	10.08706538	C
atom	14.24901556	7.71903332	10.72578116	C
atom	13.37477451	6.89320874	10.01516525	C
atom	14.08941989	8.08838720	6.43689825	C
atom	14.35976894	7.15235400	5.92615509	H
atom	14.77262563	8.87170461	6.09091739	H
atom	13.07704228	8.34989030	6.09769499	H
atom	15.99240924	9.53842426	10.88511554	C
atom	16.80342755	9.94300508	10.26790152	H
atom	16.43936695	9.00174695	11.73169412	H
atom	15.43718491	10.39267292	11.30055149	H
atom	12.48697351	5.90880466	10.72505988	C
atom	11.42272590	6.13130073	10.56150972	H
atom	12.67101476	5.92940201	11.80471775	H
atom	12.65936144	4.88451821	10.36591340	H
atom	11.47328622	3.44993056	5.78413945	C
atom	11.08691747	2.21934915	6.33370620	C

atom	10.94521253	1.13636337	5.45757688	C
atom	11.14935895	1.26234133	4.08053633	C
atom	11.47750141	2.52370515	3.57130324	C
atom	11.63879562	3.63443410	4.40038156	C
atom	10.80089237	2.06761681	7.80229168	C
atom	11.67467696	2.32586479	8.41539285	H
atom	10.50786674	1.03808224	8.03582720	H
atom	9.98196635	2.72996395	8.11792229	H
atom	11.02399040	0.08022528	3.15821153	C
atom	10.17888046	0.20454705	2.46614085	H
atom	10.86653583	-0.85179850	3.71353282	H
atom	11.92647453	-0.03507440	2.54019116	H
atom	11.95578804	4.98450111	3.81637661	C
atom	11.05189869	5.60838468	3.75086358	H
atom	12.36016676	4.88301827	2.80305991	H
atom	12.67968247	5.54172087	4.42389749	H
atom	14.47421073	1.78065661	5.34549942	C
atom	14.56243399	1.13158738	4.12921167	C
atom	14.88302947	1.85929547	2.96525996	C
atom	15.14779355	3.23417626	3.13513992	C
atom	15.04365554	3.80237823	4.39222163	C
atom	16.28749662	1.98947802	9.05766710	C
atom	17.38278706	1.22013518	9.40278898	C
atom	18.56173711	1.28011651	8.62890934	C
atom	18.53977231	2.15107565	7.51910657	C
atom	17.40120297	2.88549405	7.24208463	C
atom	14.53234572	3.96277520	7.51946642	Ir
atom	14.38640306	4.31678052	9.06135291	H

atom	13.64984110	2.68838106	7.89736121	H
atom	14.68997982	3.10854653	5.49837320	N
atom	16.27305541	2.82315964	7.98858873	N
atom	12.47646106	6.17531140	7.85268146	N
atom	11.64667518	4.59006668	6.64367437	N
atom	14.90471505	1.24462579	1.69874254	C
atom	14.86699600	0.07215815	-0.66160020	C
atom	14.55805231	-1.30106817	-0.76794033	C
atom	14.53458950	-1.91598497	-2.01465792	C
atom	14.81680745	-1.17868906	-3.16815543	C
atom	15.12443865	0.18147986	-3.07289518	C
atom	15.15095926	0.80804683	-1.83200950	C
atom	14.88874285	0.70246082	0.60432307	C
atom	19.69729607	0.51297636	8.94929674	C
atom	20.68053020	-0.15371342	9.23338299	C
atom	21.81799393	-0.92575132	9.56464149	C
atom	21.79302799	-1.78895446	10.68127417	C
atom	22.91443407	-2.54517635	11.00281448	C
atom	24.07120159	-2.45474474	10.22336930	C
atom	24.10558668	-1.60264199	9.11584752	C
atom	22.99071350	-0.84136407	8.78362203	C
atom	15.53441485	5.30606855	6.91004032	H
atom	15.42779518	5.42693174	7.78492671	H
atom	9.66138550	5.40399010	6.38184527	H
atom	10.73152481	7.44659400	7.95004657	H
atom	10.65878005	0.16669897	5.86866392	H
atom	11.62766336	2.64428905	2.49689467	H
atom	15.64606310	9.47401653	8.17933407	H

atom	14.28113286	7.63320449	11.81340668	H
atom	15.22833212	4.86572014	4.53431006	H
atom	14.19428471	1.24091454	6.24630742	H
atom	14.35284855	0.06600507	4.07122340	H
atom	15.41846502	3.85302517	2.28231055	H
atom	14.34133574	-1.86891231	0.13573243	H
atom	14.29597499	-2.97631179	-2.08954302	H
atom	14.79760060	-1.66506383	-4.14284390	H
atom	15.34511613	0.75521320	-3.97230429	H
atom	15.39052811	1.86710175	-1.74932501	H
atom	17.37400585	3.55844169	6.38722429	H
atom	19.41420918	2.25014766	6.87971334	H
atom	23.00936971	-0.17468585	7.92282271	H
atom	20.88814965	-1.85296089	11.28366334	H
atom	22.88862183	-3.20918323	11.86609884	H
atom	24.94758506	-3.04909017	10.47975781	H
atom	25.00779737	-1.53242908	8.50928288	H
atom	15.37263463	1.95816871	9.64360375	H
atom	17.33016679	0.57046788	10.27367419	H

PTC 5 – 0.87 eV:

atom	12.93849121	5.12851276	6.81161236	C
atom	10.71089316	5.43359766	6.44862987	C
atom	11.30955558	6.64123431	6.31055264	C
atom	13.59984447	7.53944211	6.55531997	C
atom	14.31794024	7.84292832	5.38749011	C
atom	15.20697936	8.92250841	5.43956184	C
atom	15.35433984	9.70899486	6.58717170	C
atom	14.58264743	9.39451386	7.71131999	C

atom	13.70053763	8.31333013	7.72479068	C
atom	14.10826323	7.07442927	4.10991464	C
atom	14.17907599	5.98767528	4.25015913	H
atom	14.84393748	7.37069461	3.35418083	H
atom	13.10868682	7.27179677	3.69522996	H
atom	16.30119779	10.87667606	6.61449609	C
atom	17.05156069	10.80768061	5.81790043	H
atom	16.82231196	10.94516868	7.57817250	H
atom	15.75656390	11.82194829	6.47235737	H
atom	12.88355474	8.00114780	8.94859340	C
atom	11.81379729	8.19211845	8.78042303	H
atom	13.20421340	8.62205553	9.79166938	H
atom	12.97743953	6.94727579	9.24354453	H
atom	11.41603275	3.13607803	7.03002159	C
atom	11.02324308	2.78455963	8.32959310	C
atom	10.75329083	1.43496498	8.58093516	C
atom	10.84626241	0.46218208	7.58359838	C
atom	11.20192127	0.86823196	6.29024987	C
atom	11.48014778	2.20092915	5.98206808	C
atom	10.86687371	3.80938109	9.41852198	C
atom	11.62794353	4.59567432	9.36149963	H
atom	10.93709270	3.34024673	10.40610482	H
atom	9.88548304	4.30319435	9.35257614	H
atom	10.54065735	-0.98175129	7.87718368	C
atom	9.57617739	-1.27541138	7.43762112	H
atom	10.48293436	-1.17057779	8.95568417	H
atom	11.30244069	-1.64879478	7.45194067	H
atom	11.82338565	2.61427309	4.57865218	C

atom	11.15390135	3.40591359	4.21390082	H
atom	11.74289564	1.76341275	3.89336876	H
atom	12.84767303	3.00914592	4.51484739	H
atom	16.75778363	8.37985554	10.59098389	C
atom	15.99554009	7.23537682	10.37839762	C
atom	16.12578739	6.53758812	9.16076315	C
atom	17.05680797	7.04625068	8.23994779	C
atom	17.78160784	8.18966857	8.56175683	C
atom	16.39464852	1.66547039	6.86676384	C
atom	17.43304373	0.76549883	7.00900062	C
atom	18.62009116	1.15399898	7.66799729	C
atom	18.66299450	2.47805155	8.15288151	C
atom	17.57576878	3.31444846	7.97544227	C
atom	14.71390871	4.21470384	7.10655977	Ir
atom	13.82051991	2.96507884	7.49077963	H
atom	14.46259162	3.53177641	5.67461548	H
atom	17.63975472	8.87066325	9.70667027	N
atom	15.81157595	5.13071832	6.04002480	H
atom	16.44282233	2.93510517	7.34045430	N
atom	12.66460220	6.44636963	6.54022182	N
atom	11.70763847	4.51966149	6.75410820	N
atom	9.67553857	5.13324087	6.36216697	H
atom	10.90937708	7.61848663	6.07695763	H
atom	11.25345277	0.12551856	5.49191592	H
atom	10.46763991	1.14091675	9.59202794	H
atom	15.78686079	9.16536469	4.54746360	H
atom	14.68819305	9.99548519	8.61556482	H
atom	15.33052516	5.36565433	8.92675516	C

atom	14.67281398	4.35231802	9.31486748	C
atom	14.14048001	3.48234819	10.32378711	C
atom	13.87827544	2.12082068	10.09214205	C
atom	13.38198420	1.31485675	11.11175609	C
atom	13.12921532	1.85145067	12.37579907	C
atom	13.88751888	4.01390283	11.60736343	C
atom	13.38409078	3.20455666	12.61907524	C
atom	19.69983405	0.26782522	7.83147509	C
atom	20.63586806	-0.50416943	7.97404710	C
atom	21.71864145	-1.39749007	8.13972646	C
atom	21.63828584	-2.71552645	7.64034384	C
atom	22.70645955	-3.58939863	7.80665309	C
atom	23.86362009	-3.16785646	8.46804048	C
atom	23.95251611	-1.86463212	8.96584356	C
atom	22.89139470	-0.98094372	8.80615456	C
atom	22.95206996	0.03603053	9.19058480	H
atom	24.69816220	-3.85652982	8.59562504	H
atom	24.85508325	-1.53756914	9.48072949	H
atom	20.73329993	-3.03524754	7.12603138	H
atom	22.63893391	-4.60521013	7.41896308	H
atom	15.47643932	1.38383459	6.35757365	H
atom	17.33022881	-0.24110002	6.60985590	H
atom	19.54611021	2.84736984	8.66948808	H
atom	17.59815986	4.33022356	8.36177666	H
atom	16.65161120	8.93904620	11.52356957	H
atom	15.28950267	6.89831106	11.13487851	H
atom	17.20732539	6.57161609	7.27264129	H
atom	18.50467342	8.59303608	7.84909655	H

atom	14.07717110	5.06945208	11.79548820	H
atom	12.73460755	1.21920961	13.17043184	H
atom	13.18681720	3.62998295	13.60247479	H
atom	14.05732367	1.70455927	9.10293085	H
atom	13.18393452	0.26160612	10.91543979	H
atom	15.36300419	5.75453266	6.42106671	H

5. Full matrix of the Hamiltonian

	$\lvert S_0^H S_0^C\rangle$	$\lvert T_0^H T_0^C\rangle$	$\lvert T_+^H T_-^C\rangle$	$\lvert T_-^H T_+^C\rangle$	$\lvert T_+^H T_+^C\rangle$	$\lvert T_-^H T_-^C\rangle$	$\lvert T_0^H T_+^C\rangle$	$\lvert T_+^H T_0^C\rangle$
$\lvert S_0^H S_0^C\rangle$	$-(J_{HH}+J_{CC})$	$\frac{\Delta J_{near}-\Delta J_{far}}{4}$	$\frac{\Delta J_{far}-\Delta J_{near}}{4}$	$\frac{\Delta J_{far}-\Delta J_{near}}{4}$	0	0	0	0
$\lvert T_0^H T_0^C\rangle$	$\frac{\Delta J_{near}-\Delta J_{far}}{4}$	0	$\frac{\Sigma J_{near}+\Sigma J_{far}}{4}$	$\frac{\Sigma J_{near}+\Sigma J_{far}}{4}$	0	0	0	0
$\lvert T_+^H T_-^C\rangle$	$\frac{\Delta J_{far}-\Delta J_{near}}{4}$	$\frac{\Sigma J_{near}+\Sigma J_{far}}{4}$	$(\nu_H-\nu_C)-\frac{\Sigma J_{near}+\Sigma J_{far}}{4}$	0	0	0	0	0
$\lvert T_-^H T_+^C\rangle$	$\frac{\Delta J_{far}-\Delta J_{near}}{4}$	$\frac{\Sigma J_{near}+\Sigma J_{far}}{4}$	0	$(\nu_C-\nu_H)+\frac{\Sigma J_{near}+\Sigma J_{far}}{4}$	0	0	0	0
$\lvert T_+^H T_+^C\rangle$	0	0	0	0	$\frac{\Sigma J_{near}+\Sigma J_{far}}{4}+\nu_H+\nu_C$	0	0	0
$\lvert T_-^H T_-^C\rangle$	0	0	0	0	0	$\frac{\Sigma J_{near}+\Sigma J_{far}}{4}-(\nu_H+\nu_C)$	0	0
$\lvert T_0^H T_+^C\rangle$	0	0	0	0	0	0	ν_C	$\frac{\Sigma J_{near}+\Sigma J_{far}}{4}$
$\lvert T_+^H T_0^C\rangle$	0	0	0	0	0	0	$\frac{\Sigma J_{near}+\Sigma J_{far}}{4}$	ν_H
$\lvert T_0^H T_-^C\rangle$	0	0	0	0	0	0	0	0
$\lvert T_-^H T_0^C\rangle$	0	0	0	0	0	0	0	0
$\lvert S_0^H T_0^C\rangle$	0	0	$\frac{\Delta J_{far}+\Delta J_{near}}{4}$	$\frac{-\Delta J_{far}-\Delta J_{near}}{4}$	0	0	0	0
$\lvert T_0^H S_0^C\rangle$	0	0	$\frac{\Sigma J_{far}-\Sigma J_{near}}{4}$	$\frac{\Sigma J_{near}-\Sigma J_{far}}{4}$	0	0	0	0
$\lvert S_0^H T_+^C\rangle$	0	0	0	0	0	0	$\frac{-\Delta J_{far}-\Delta J_{near}}{4}$	$\frac{\Delta J_{far}+\Delta J_{near}}{4}$
$\lvert T_+^H S_0^C\rangle$	0	0	0	0	0	0	$\frac{\Sigma J_{near}-\Sigma J_{far}}{4}$	$\frac{\Sigma J_{far}-\Sigma J_{near}}{4}$
$\lvert S_0^H T_-^C\rangle$	0	0	0	0	0	0	0	0
$\lvert T_-^H S_0^C\rangle$	0	0	0	0	0	0	0	0

	$\lvert T_0^H T_-^C\rangle$	$\lvert T_-^H T_0^C\rangle$	$\lvert S_0^H T_0^C\rangle$	$\lvert T_0^H S_0^C\rangle$	$\lvert S_0^H T_+^C\rangle$	$\lvert T_+^H S_0^C\rangle$	$\lvert S_0^H T_-^C\rangle$	$\lvert T_-^H S_0^C\rangle$
$\lvert S_0^H S_0^C\rangle$	0	0	0	0	0	0	0	0
$\lvert T_0^H T_0^C\rangle$	0	0	0	0	0	0	0	0
$\lvert T_+^H T_-^C\rangle$	0	0	$\frac{\Delta J_{far}+\Delta J_{near}}{4}$	$\frac{\Sigma J_{far}-\Sigma J_{near}}{4}$	0	0	0	0
$\lvert T_-^H T_+^C\rangle$	0	0	$\frac{-\Delta J_{far}-\Delta J_{near}}{4}$	$\frac{\Sigma J_{near}-\Sigma J_{far}}{4}$	0	0	0	0
$\lvert T_+^H T_+^C\rangle$	0	0	0	0	0	0	0	0
$\lvert T_-^H T_-^C\rangle$	0	0	0	0	0	0	0	0
$\lvert T_0^H T_+^C\rangle$	0	0	0	0	$\frac{-\Delta J_{far}-\Delta J_{near}}{4}$	$\frac{\Sigma J_{near}-\Sigma J_{far}}{4}$	0	0
$\lvert T_+^H T_0^C\rangle$	0	0	0	0	$\frac{\Delta J_{far}+\Delta J_{near}}{4}$	$\frac{\Sigma J_{far}-\Sigma J_{near}}{4}$	0	0
$\lvert T_0^H T_-^C\rangle$	$-\nu_C$	$\frac{\Sigma J_{near}+\Sigma J_{far}}{4}$	0	0	0	0	$\frac{\Delta J_{far}+\Delta J_{near}}{4}$	$\frac{\Sigma J_{far}-\Sigma J_{near}}{4}$
$\lvert T_-^H T_0^C\rangle$	$\frac{\Sigma J_{near}+\Sigma J_{far}}{4}$	$-\nu_H$	0	0	0	0	$\frac{-\Delta J_{far}-\Delta J_{near}}{4}$	$\frac{\Sigma J_{near}-\Sigma J_{far}}{4}$
$\lvert S_0^H T_0^C\rangle$	0	0	$-J_{HH}$	$\frac{\Delta J_{near}-\Delta J_{far}}{4}$	0	0	0	0
$\lvert T_0^H S_0^C\rangle$	0	0	$\frac{\Delta J_{near}-\Delta J_{far}}{4}$	$-J_{CC}$	0	0	0	0
$\lvert S_0^H T_+^C\rangle$	0	0	0	0	$-J_{HH}+\nu_C$	$\frac{\Delta J_{near}-\Delta J_{far}}{4}$	0	0
$\lvert T_+^H S_0^C\rangle$	0	0	0	0	$\frac{\Delta J_{near}-\Delta J_{far}}{4}$	$-J_{CC}+\nu_H$	0	0
$\lvert S_0^H T_-^C\rangle$	$\frac{\Delta J_{far}+\Delta J_{near}}{4}$	$\frac{-\Delta J_{far}-\Delta J_{near}}{4}$	0	0	0	0	$-\nu_C-J_{HH}$	$\frac{\Delta J_{near}-\Delta J_{far}}{4}$
$\lvert T_-^H S_0^C\rangle$	$\frac{\Sigma J_{far}-\Sigma J_{near}}{4}$	$\frac{\Sigma J_{near}-\Sigma J_{far}}{4}$	0	0	0	0	$\frac{\Delta J_{near}-\Delta J_{far}}{4}$	$-\nu_H-J_{CC}$

References

1. Blum, V.; Gehrke, R.; Hanke, F.; Havu, P.; Havu, V.; Ren, X.; Reuter, K.; Scheffler, M. Ab initio molecular simulations with numeric atom-centered orbitals. *Comput Phys Commun* **2009,** *180* (11), 2175-2196.
2. Perdew, J. P.; Burke, K.; Ernzerhof, M. Generalized Gradient Approximation Made Simple. *Phys. Rev. Lett.* **1996,** *77* (18), 3865-3868.
3. Tkatchenko, A.; Scheffler, M. Accurate Molecular Van Der Waals Interactions from Ground-State Electron Density and Free-Atom Reference Data. *Phys. Rev. Lett.* **2009,** *102* (7), 073005.
4. Jr., T. H. D. Gaussian basis sets for use in correlated molecular calculations. I. The atoms boron through neon and hydrogen. *J. Chem. Phys.* **1989,** *90* (2), 1007-1023.
5. Deng, W.; Cheeseman, J. R.; Frisch, M. J. Calculation of Nuclear Spin−Spin Coupling Constants of Molecules with First and Second Row Atoms in Study of Basis Set Dependence. *J. Chem. Theory Comput.* **2006,** *2* (4), 1028-1037.